Article

Not peer-reviewed version

$CH_3NH_3PbBr_3$ Perovskite Single Crystal X-Ray Photon Counting Detection Based on Multi-Layer Electrodes

Songchao Wang , Hanwen Zhang , Gangyi Chen , Yuzhu Pan , Yulian Zhang , Qianqian Huang , Jinbao Chen , Xin Wang *

Posted Date: 3 April 2026

doi: 10.20944/preprints202604.0223.v1

Keywords: $CH_3NH_3PbBr_3$ single crystal; multi-layer electrode; X-ray photon counting detection

 doi:10.20944/preprints202604.0223.v1

Article

$CH_3NH_3PbBr_3$ Perovskite Single Crystal X-Ray Photon Counting Detection Based on Multi-Layer Electrodes

Songchao Wang [1,2], Hanwen Zhang [3], Gangyi Chen [2], Yuzhu Pan [4], Yulian Zhang [5], Qianqian Huang [6], Jinbao Chen [1,5] and Xin Wang [1,5,*]

[1] National Key Laboratory of Aerospace Mechanism, Nanjing University of Aeronautics and Astronautics, Nanjing 210016, China
[2] Shanghai Institute of Spacecraft Equipment, Shanghai 200000, China
[3] Shanghai Aerospace Equipments Manufacturer Co.Ltd, Shanghai 200245, China
[4] Key Laboratory of Semiconductor Display Materials and Chips, Suzhou Institute of Nano-Tech and Nano-Bionics, Chinese Academy of Sciences, Suzhou 215123, China
[5] College of Physics, Nanjing University of Aeronautics and Astronautics, Nanjing 210016, China
[6] School of Information Technology, Jiangsu Open University, Nanjing 210017, China
* Correspondence: xin-wang@nuaa.edu.cn

Abstract

$CH_3NH_3PbBr_3$ ($MAPbBr_3$) single crystals have shown great potential in X/γ-ray detection. However, stable electrodes for $MAPbBr_3$ single crystals still remains challenging. In this work, multi-layer electrodes including Au, Au/Ti and Au/Pt/Ti are investigated. Through I-V characterization, Au/Pt/Ti shows Ohmic contact behavior and lowest dark current. The potential contact is also confirmed by Kelvin force probe. Based on this low noise electrodes, 59.5 keV monochromatic X-ray photon counting detection and imaging is demonstrated. This work provides useful information for electrodes design in lead halide perovskites-based optoelectronic devices.

Keywords: $CH_3NH_3PbBr_3$ single crystal; multi-layer electrode; X-ray photon counting detection

1. Introduction

X-ray detection technologies play a critical role in a wide range of applications, including medical imaging, industrial non-destructive testing, and security check [1–3]. Among various detection modalities, photon counting detection has emerged as a next-generation paradigm due to its superior capabilities in energy resolution, contrast-to-noise ratio, and reduced radiation dose compared to conventional energy-integrating systems [4–9]. The success of photon counting detection, however, heavily relies on the availability of high-performance semiconductor materials that exhibit both efficient X-ray absorption and excellent charge transport properties [10].

In recent years, lead halide perovskites have garnered significant attention as promising candidates for X-ray detection, owing to their exceptional optoelectronic properties, including high atomic numbers, large mobility-lifetime (μτ) products, and low-cost solution-processability [11–13]. Among kinds of lead halide perovskites, methylammonium lead bromide ($MAPbBr_3$, $MA=CH_3NH_3$) stands out as a particularly attractive material for X-ray photon counting applications, as it combines strong X-ray attenuation capability with high resistivity and quick growth speed from solution precursor [14–16]. These attributes have enabled MAPbBr3 single crystals based X-ray detectors to achieve impressive sensitivity and lowest detection limits, positioning them as viable alternatives to conventional materials such as amorphous selenium, cadmium zinc telluride, and silicon [17–20].

Despite these advances, the application of $MAPbBr_3$ single crystals in X-ray photon counting detection remains challenging, primarily due to issues related to device stability, high dark current,

 doi:10.20944/preprints202604.0223.v1

and charge trapping under high electric fields [21–23]. The electrode configuration plays a crucial role in governing charge collection efficiency and suppressing dark current in perovskite X-ray detectors. Conventional single-layer metal electrodes such as Au, Ag, Ti and Ga, often suffer from inefficient charge extraction, interfacial reactions with the $MAPbBr_3$ single crystals, and increased leakage currents, limiting the detector's ability to operate stably under sustained high bias and X-ray irradiation [24–27]. While previous studies have largely focused on optimizing the active layer composition and interface engineering, relatively little attention has been paid to the rational design of multi-layer electrode architectures tailored for photon counting mode, particularly in the context of $MAPbBr_3$ single crystal-based devices [5,28].

To address these limitations, we propose the implementation of multi-layer electrode structures employing Au/$MAPbBr_3$/Au, Au/Ti/$MAPbBr_3$/Ti/Au and Au/Pt/Ti$MAPbBr_3$/Ti/Pt/Au configurations. These multi-layer architectures are designed to combine the advantages of each metal layer: Ti serves as an adhesion layer, where Ti-N bonds formed at the interface of $MAPbBr_3$/Ti; Pt functions as a isolating layer to mitigate interfacial reactions and ion migration; while Au ensures high conductivity. By systematically comparing the performance of $MAPbBr_3$ X-ray detectors with single-layer and multi-layer electrodes, we investigate the influence of electrode architecture on 59.5 keV photon-counting detection and imaging. In this work, low activity ^{241}Am radioactive gamma-ray sources were used as low dose monochromatic X-ray source.

Our results demonstrated that the multi-layer electrode strategy, particularly the Au/Pt/Ti/$MAPbBr_3$/Ti/Pt/Au configuration, significantly enhances both the detection performance and long-term stability of $MAPbBr_3$-based photon counting X-ray detectors. The improved charge extraction, suppressed dark current, and mitigated interfacial degradation achieved through this rational electrode design offer a promising pathway toward practical and reliable perovskite-based photon counting X-ray detection systems.

2. Materials and Methods

Materials: Lead bromide (PbBr2; 99%) and methylammonium bromide (MABr), were purchased from Sigma Aldrich, USA. Dimethyl sulfoxide (DMSO) and dimethylformamide (DMF) were obtained from Aladdin. Metallic gold were purchased from Chinese reagent, China. All commercial products were used as received.

Growth of $MAPbBr_3$ perovskite single crystals. High-quality $MAPbBr_3$ perovskite single crystals were grown by inverse temperature crystallization [29–31]. Specifically, 1 M MABr and 1 M $PbBr_2$ were dissolved in DMF solution. The solutions were filtered through a PTFE filter with a 30 μm pore size. The filtrate was then transferred to a culture dish, which was placed on a programmable heating station (IKA-RET control-visc) and the growth temperature is 65 to 85 ℃. For the metal electrodes: electrodes were deposited face of $MAPbBr_3$ perovskite single crystals by a metal mask under a vacuum of 6×10^{-4} Pa.

Characterization of the $MAPbBr_3$ perovskite single crystals. X-ray diffraction (XRD) patterns were obtained using an X'TRA system with a Cu target (Switzerland). Optical absorption spectra were measured by UV-vis spectroscopy range from 300 to 2000 nm (Lab Tech Bluestar, USA). The ultraviolet photoelectron spectroscopy (UPS) were obtained using a PHI 5000 VersaProbe (Japan). The PL and PL decay processes were measured using a SpectraMax instrument (UK). The kelvin force probe microscopy was using a Dimension Icon (Bruker, German). For the response time measurement: ^{241}Am was used as the radioactive source, a high voltage bias (0-50V) was applied on the device, the signal was input into a pre-amplifier(142PC, USA). The response to each alpha particle was traced using an Keysight oscilloscope (DMOX4054A, USA). Characterization of current–voltage were measured using a Keithley 4200SC semiconductor analyzer (USA).

Set-up of the X-ray photon-counting read-out circuits. The pre-amplifier 142PC was purchased from ORTEC (USA). The shaping amplifier and baseline restorer were purchased from CREMAT (USA). The high voltage and low voltage DC source were purchased from DONGWEN HIGH VOLTAGE (China). And the multi-channel analyzer was purchased from AP Techno (Japan).

 doi:10.20944/preprints202604.0223.v1

3. Results

As shown in Figure 1, the energy band of $MAPbBr_3$ single crystal was investigated. The band gap was fitted of 2.1 eV by Talc plot (Figure S1). And the valance band maximum was measured of 5.7 eV by UPS (Figure S2). And the work function of Au, Pt, Ti were chosen to be 5.1 eV, 5.3 eV and 4.3 eV from published work, respectively. Figure 1b shows the structure of detectors made of $MAPbBr_3$ single crystals with different electrodes, including Au/$MAPbBr_3$/Au, Au/Ti/$MAPbBr_3$/Ti/Au and Au/Pt/Ti/$MAPbBr_3$/Ti/Pt/Au. Interdigitated electrode was chosen as shown in Figure 1c, the thickness of three type of electrodes was 200 nm. Here, ^{241}Am radioactive sources which emit 59.5 keV photons were used as monochromatic X-ray source. As shown in Figure 1d, the 59.5 keV monochromatic X-ray photons would incident into the detectors, while high voltage bias and ground would connect to each electrode, respectively.

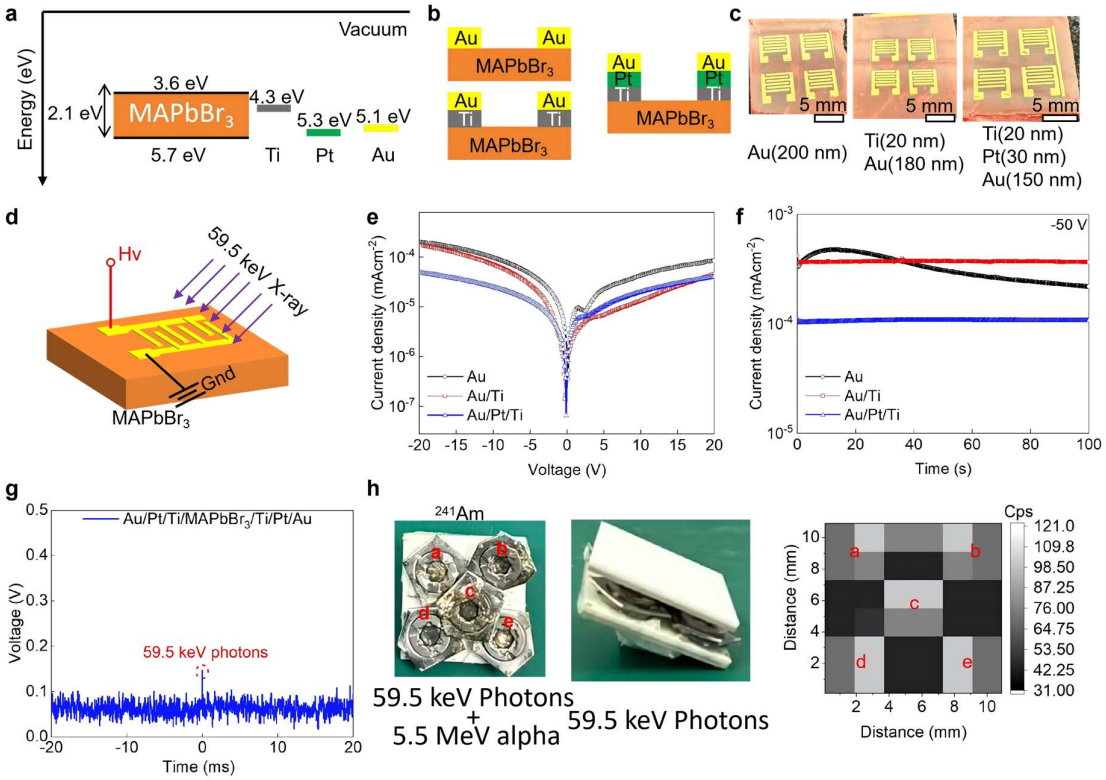

Figure 1. a. Energy band diagram of $MAPbBr_3$ single crystal and different metals. **b.** Device structure. **c.** Optical photo of devices with different electrodes. **d.** Diagram of the device under bias and 59.5 keV radiation. **e.** I-V characterization of $MAPbBr_3$ single crystals with different electrodes. **f.** I-T characterization of $MAPbBr_3$ single crystals with different electrodes under -50 V. **g.** 59.5 keV photon response of Au/Pt/Ti/$MAPbBr_3$/Ti/Pt/Au. **h.** Image of five ^{241}Am source.

Figure 1e shows the current density- voltage characterization of detectors with different electrode structures, the Au/Pt/Ti multi-layer electrodes shows nearly linear behavior, while Au electrode or Au/Ti electrode show back-to-back Schottky behavior. The Au/Pt/Ti multi-layer seems to form more Ohmic contact with $MAPbBr_3$ single crystal. Further, the dark current density under -50 V bias was investigated in Figure 1f, the Au/Pt/Ti multi-layer device shows lowest dark current of 107 $nAcm^{-2}$, which was much lower than Au/Ti device and Au device of 372 $nAcm^{-2}$ 227~445 $nAcm^{-2}$, respectively.

Owning to the low and stable dark current, Au/Pt/Ti multi-layer device was used to detect 59.5 keV photons. As shown in Figure 1g, a 59.5 keV photon induced potential pulse could be clearly

 doi:10.20944/preprints202604.0223.v1

observed. While for Au/Ti multi-layer device and Au device, the noise were too large to discriminate the useful signal(Figure S3). And the alpha particles response was shown in Figure S4. Further, we use five ^{241}Am radioactive sources as five point X-ray source, a 1 mm thickness Al_2O_3 ceramic sheet was used to filter alpha particles and only 59.5 keV photons could transmit as shown in Figure 1h. Based on the count per second of Au/Pt/Ti multi-layer device in different location, we successfully realize X-ray photon counting image. The five ^{241}Am radioactive sources only emit nearly 1000 59.5 keV photons per second, and the photon injection power is only 100 $cm^{-2}s^{-1}$. Based on $D_{air}=\varphi\times(\frac{\mu_{en}}{\varrho})\times E$, where D_{air} is the dose rate, φ is the photon injection rate, E is the energy of each photon and $\frac{\mu_{en}}{\varrho}$ is the mass energy absorption coefficient, which is 0.0303 cm^2g^{-1} for air [32]. As a result, the dose rate was only 0.03 $nGys^{-1}$, which is much lower to the lowest detectable dose rate in energy-integrating X-ray detectors.

4. Discussion

After multi-layer electrodes deposition, we further confirmed the surface property of $MAPbBr_3$ single crystals. Since the deposition temperature for metal Pt is much higher than Au, the high temperature vaporized Pt or Au may destroy the surfaces of $MAPbBr_3$ single crystals. As shown in Figure 2a, the surface property of $MAPbBr_3$ single crystals was first investigated by the X-ray diffraction. The full width half height (FWHM) for 30.080 degree was 0.2, 0.2 and 0.18 degree for Au, Au/Ti and Au/Pt/Ti device, respectively. The X-ray diffraction shows that the crystallization quality of three $MAPbBr_3$ single crystals after electrodes deposition was close. Further, photoluminescence of three $MAPbBr_3$ single crystals after electrodes deposition was investigated in Figure 2b. The peak of the photoluminescence located at 530 nm, and the photoluminescence intensity was nearly equal. And the time-resolved photoluminescence of 530 nm was further investigate in Figure 2c. Through exponential decay fitting, the surface lifetime was 0.32±0.02, 0.37±0.02 and 0.35±0.04 μs and the bulk lifetime was 10.5±3.7, 10.5±2.3 and 14.2±4.5 μs for Au, Au/Ti and Au/Pt/Ti device, respectively. As result, the dark current density and noise behavior were attributed to the different electrodes not to the crystallization quality differences of $MAPbBr_3$ single crystals.

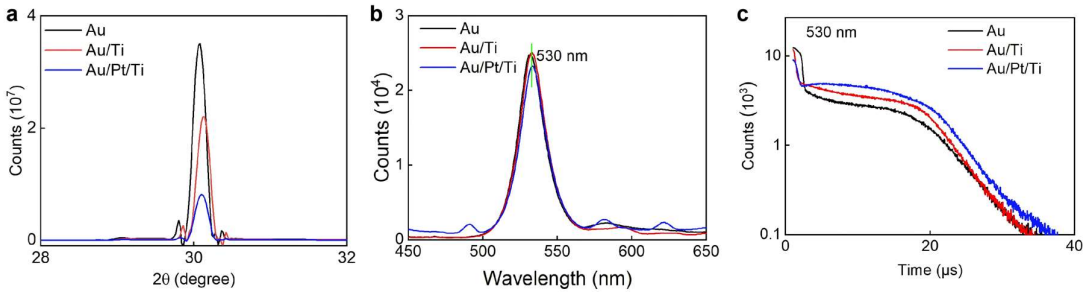

Figure 2. Characterization of $MAPbBr_3$ single crystals with different electrodes. a. X-ray diffraction. b. Photoluminescence under 350 nm. c. Time resolved photoluminescence of 530 nm.

 doi:10.20944/preprints202604.0223.v1

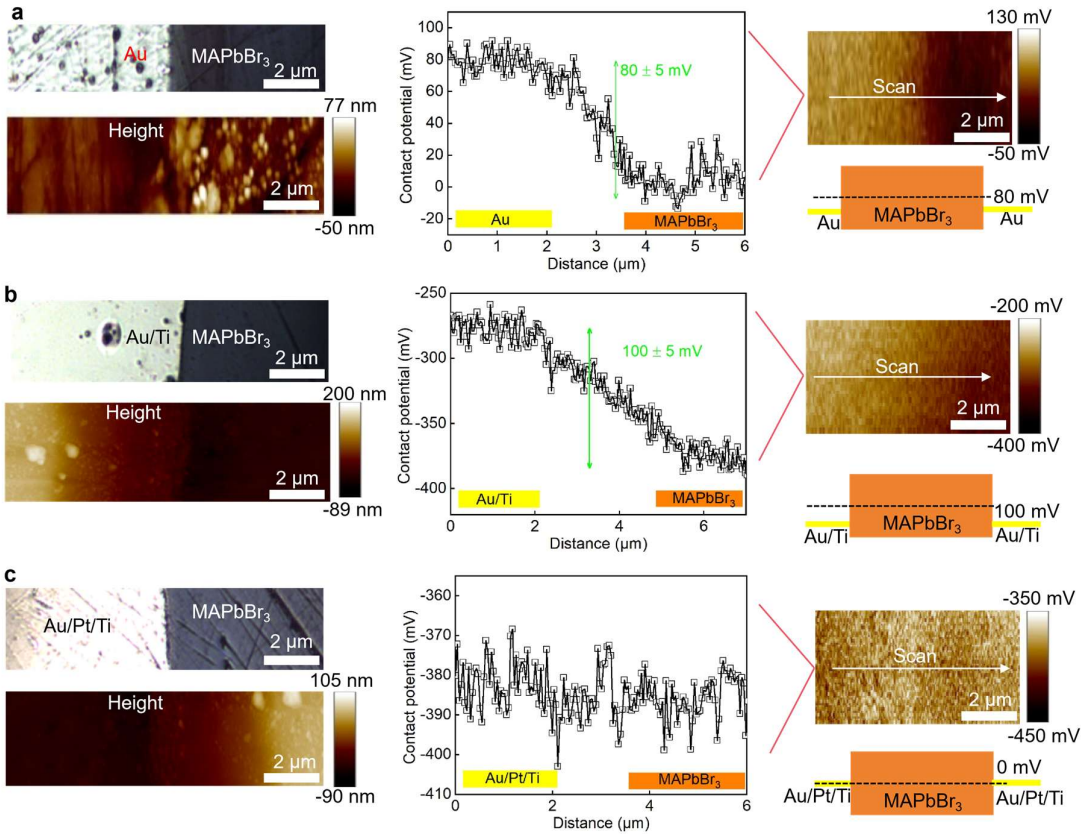

Figure 3. Kelvin force microscopy results. a. Au/MAPbBr3. b. Au/Ti/MAPbBr3. c. Au/Pt/Ti/MAPbBr3.

To further understand the metal- MAPbBr3 single crystal contact, here, Kelvin Force Microscopy (KFM) was used to measure the contact potential of different electrodes. The KFM results for Au device was shown in Figure 3a, the roughness was 5±1 and 25±3 nm for Au area and MAPbBr3 single crystal region, respectively. And the contact potential was measured of 0.15±0.02 V, resulted in a energy barrier of 80 mV in Au-MAPbBr3 interface. Similarly, for Au/Ti device, the roughness was 3±1 and 15±3 nm for Au/Ti area and MAPbBr3 single crystal region, respectively. Further, the contact potential was measured of 0.15±0.02 V, resulted in a energy barrier of 100 mV in Au/Ti-MAPbBr3 interface. For the Au/Pt/Ti device, the the roughness was 3±1 and 15±3 nm for Au/Ti area and MAPbBr3 single crystal region, respectively. What's interesting, we can not observe clear potential difference between Au/Pt/Ti and MAPbBr3 single crystal. It also explained the Ohmic behavior as shown in current density-voltage characterization.

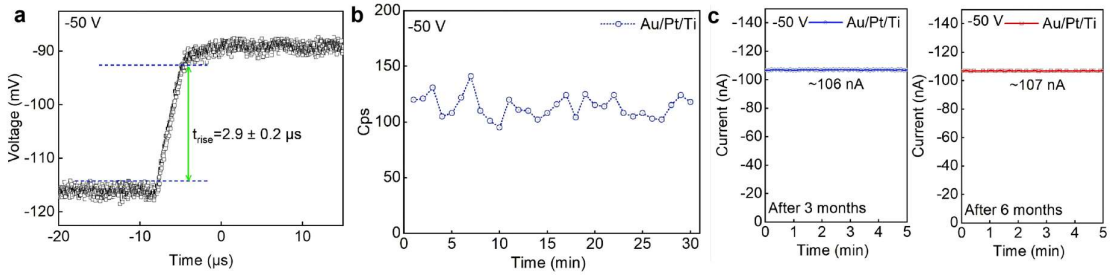

Figure 4. a. Response time to single 59.5 keV photon. **b.** Count per second stability. **c.** Long time stability of Au/PT/Ti/MAPbBr3/Ti/Pt/Au.

 doi:10.20944/preprints202604.0223.v1

As shown in Figure 4a, the response speed for Au/Pt/Ti device, at -50 V bias, the response speed reached 2.9±0.2μs, corresponding to the maximum count rate of 34.4k s^{-1}. As shown in Figure 4b, the counting stability of Au/Pt/Ti device was 110±15 for 59.5 keV photons for 30 minutes, demonstrating the not bad counting stability. The Au/Pt/Ti device was also very stable. As shown in Figure 4c, the dark current after 6 months (107 nA) maintained almost the same dark current after 3 months(106 nA).

5. Conclusions

In this work, multi-layer electrodes including Au, Au/Ti and Au/Pt/Ti were investigated. Au and Au/Ti would form energy barriers when contact with $MAPbBr_3$ single crystals, while Au/Pt/Ti could form Ohmic contact with $MAPbBr_3$ single crystals. Au/Pt/Ti multi-layer electrode shows lowest dark current and noise, which enable 59.5 keV photon counting detection and imaging. This work provided useful information about the electrodes structure for lead halide perovskites based optoelectronic devices.

Supplementary Materials: The following supporting information can be downloaded at the website of this paper posted on Preprints.org, **Figure S1:** Absorption curve of $MAPbBr_3$ single crystal;.**Figure S2:** UPS result of $MAPbBr_3$ single crystal.**Figure S3:** Noise of Au, Au/Ti and Au/Pt/Ti under -50 V bias.**Figure S4:** Alpha response of Au/Pt/Ti device.

Author Contributions: Conceptualization, X.W. and S.W.; methodology, X.W.; formal analysis, H.Z.; investigation, Y.P.; resources, Q.H.; writing—original draft preparation, W.X.; writing; All the author make comments on the manuscript.

Funding: This work is financially supported by National Natural Science Foundation of China (grant numbers 12375306, 12305201 and 12274224).

Institutional Review Board Statement: Not applicable.

Informed Consent Statement: Not applicable.

Data Availability Statement: The original contributions presented in this study are included in the article/supplementary material. Further inquiries can be directed to the corresponding author(s).

Acknowledgments: We can acknowledge the support given by Yuwei Li, who helped us to do the UPS experiments.

Conflicts of Interest: The authors declare no conflicts of interest.

References

1. Liu, Z.; Wang, X.; Lei, W., Solution-processed epitaxial growth of PIN photodiodes made of MAPbBr3 single crystals for high energy resolution gamma-ray spectroscopy. *Journal of Materials Chemistry C* **2025,** 13, (47), 23467-23474.
2. Park, A.; Park, B.; Seo, J.; Byun, J.; Park, S.-J.; Yoon, S.-P.; Ko, J.; Kim, J.; Lee, W.; Lee, M.-J., Exploration on high-energy and high-dose rate X-ray detection with Bridgman-grown $CsPbBr_3$ single crystal. *Nuclear Engineering and Technology* **2025,** 57, (11), 103799.
3. Peng, J.; Xia, C. Q.; Xu, Y.; Li, R.; Cui, L.; Clegg, J. K.; Herz, L. M.; Johnston, M. B.; Lin, Q., Crystallization of CsPbBr3 single crystals in water for X-ray detection. *Nature Communications* **2021,** 12, (1), 1531.
4. Li, M.; Wang, S.; Wood, A.; Yeager, J. D.; Stepanoff, S. P.; Adler, J. C.; Shi, Z.; Wang, J.; Li, Z.; Wolfe, D. E.; Huang, J., Defect repairing in lead bromide perovskite single crystals with biasing and bromine for X-ray photon-counting detectors. *Nature Materials* **2025**,24, 1993-2000.
5. Sakhatskyi, K.; Turedi, B.; Matt, G. J.; Wu, E.; Sakhatska, A.; Bartosh, V.; Lintangpradipto, M. N.; Naphade, R.; Shorubalko, I.; Mohammed, O. F.; Yakunin, S.; Bakr, O. M.; Kovalenko, M. V., Stable perovskite single-crystal X-ray imaging detectors with single-photon sensitivity. *Nature Photonics* **2023,** 17, (6), 510-517.

 doi:10.20944/preprints202604.0223.v1

6. Yang, Y.; Chen, X.; Jia, Z.; Liu, Y.; Lin, Q., Device Engineering of Bismuth-Based Chalcogenides for Low-Noise, Near-Infrared Photon-Counting. *ACS Materials Letters* **2025,** 7, (9), 3159-3166.
7. Zhou, Y.; Fei, C.; Uddin, M. A.; Zhao, L.; Ni, Z.; Huang, J., Self-powered perovskite photon-counting detectors. *Nature* **2023,** 616, (7958), 712-718.
8. Rodesch, P.-A.; Richtsmeier, D.; Guliyev, E.; Iniewski, K.; Bazalova-Carter, M., Comparison of Threshold Energy Calibrations of a Photon-Counting Detector and Impact on CT Reconstruction. *IEEE Transactions on Radiation and Plasma Medical Sciences* **2023,** 7, (3), 263-272.
9. Pan, L.; He, Y.; Klepov, V. V.; De Siena, M. C.; Kanatzidis, M. G., Perovskite CsPbBr3 Single Crystal Detector for High Flux X-Ray Photon Counting. *IEEE Transactions on Medical Imaging* **2022,** 41, (11), 3053-3061.
10. Iwanczyk, J. S.; Nygard, E.; Meirav, O.; Arenson, J.; Barber, W. C.; Hartsough, N. E.; Malakhov, N.; Wessel, J. C., Photon Counting Energy Dispersive Detector Arrays for X-ray Imaging. *IEEE Transactions on Nuclear Science* **2009,** 56, (3), 535-542.
11. Datta, A.; Fiala, J.; Motakef, S., 2D perovskite-based high spatial resolution X-ray detectors. *Scientific Reports* **2021,** 11, (1), 22897.
12. Fratelli, I.; Basiricò, L.; Ciavatti, A.; Margotti, L.; Cepić, S.; Chiari, M.; Fraboni, B., Real-Time Radiation Beam Monitoring by Flexible Perovskite Thin Film Arrays. *Advanced Science* **2024,** 11, (40), 2401124.
13. Wei, H.; Huang, J., Halide lead perovskites for ionizing radiation detection. *Nature Communications* **2019,** 10, (1), 1066.
14. Cho, Y.; Jung, H. R.; Kim, Y. S.; Kim, Y.; Park, J.; Yoon, S.; Lee, Y.; Cheon, M.; Jeong, S.-y.; Jo, W., High speed growth of MAPbBr3 single crystals via low-temperature inverting solubility: enhancement of mobility and trap density for photodetector applications. *Nanoscale* **2021,** 13, (17), 8275-8282.
15. Wang, K.-H.; Li, L.-C.; Shellaiah, M.; Wen Sun, K., Structural and Photophysical Properties of Methylammonium Lead Tribromide ($MAPbBr_3$) Single Crystals. *Scientific Reports* **2017,** 7, (1), 13643.
16. Wang, C.; Ecker, B. R.; Wei, H.; Huang, J.; Gao, Y., Environmental Surface Stability of the MAPbBr3 Single Crystal. *The Journal of Physical Chemistry C* **2018,** 122, (6), 3513-3522.
17. Eom, K.; Lee, J. T.; Oschatz, M.; Wu, F.; Kaskel, S.; Yushin, G.; Fuller, T. F., A stable lithiated silicon–chalcogen battery via synergetic chemical coupling between silicon and selenium. *Nature Communications* **2017,** 8, (1), 13888.
18. Song, Y.; Jackson, M.; Iniewski, K., Recent Results in CZT Detectors for PCCT. In 2023 IEEE Nuclear Science Symposium, Medical Imaging Conference and International Symposium on Room-Temperature Semiconductor Detectors (NSS MIC RTSD), 2023; pp 1-1.
19. Zhou, B.; Jie, W.; Wang, T.; Xu, Y.; Yang; Fan; Yin, L.; Zhang, B.; Nan, R., Growth and Characterization of Detector-Grade Cd0.9Zn0.1Te Crystals by the Traveling Heater Method with the Accelerated Crucible Rotation Technique. *Journal of Electronic Materials* **2017,** 47, (2), 1125-1130.
20. He, X.; Deng, Y.; Ouyang, D.; Zhang, N.; Wang, J.; Murthy, A. A.; Spanopoulos, I.; Islam, S. M.; Tu, Q.; Xing, G.; Li, Y.; Dravid, V. P.; Zhai, T., Recent Development of Halide Perovskite Materials and Devices for Ionizing Radiation Detection. *Chem Rev* **2023,** 123, 1207-1261.
21. Yang, Y.; Yan, Y.; Yang, M.; Choi, S.; Zhu, K.; Luther, J. M.; Beard, M. C., Low surface recombination velocity in solution-grown CH3NH3PbBr3 perovskite single crystal. *Nature Communications* **2015,** 6, (1), 7961.
22. Cao, M.; Tian, J.; Cai, Z.; Peng, L.; Yang, L.; Wei, D., Perovskite heterojunction based on CH3NH3PbBr3 single crystal for high-sensitive self-powered photodetector. *Applied Physics Letters* **2016,** 109, (23), 233303.
23. Zhang, H.; Yu, T.; Wang, C.; Jia, R.; Pirzado, A. A. A.; Wu, D.; Zhang, X.; Zhang, X.; Jie, J., High-Luminance Microsized CH3NH3PbBr3 Single-Crystal-Based Light-Emitting Diodes via a Facile Liquid-Insulator Bridging Route. *ACS Nano* **2022,** 16, (4), 6394-6403.
24. Shen, N.; Gao, T.; Ouyang, X.; Bayikadi, K. S.; Duan, Z.; Xiao, B.; He, X.; Wang, Y.; Qin, H.; Sun, Q.; Wang, L.; Lai, Y.; Liu, X.; Ren, R.; Kanatzidis, M. G.; He, Y., Enhancing Gamma-Ray Spectral Resolution in Perovskite CsPbBr3 Detectors through Dark Current Reduction with Guard Ring Electrodes. *ACS Photonics* **2024,** 11, (9), 3662-3671.

 doi:10.20944/preprints202604.0223.v1

25. Klepov, V. V.; De Siena, M. C.; Pandey, I. R.; Pan, L.; Bayikadi, K. S.; Butun, S.; Chung, D. Y.; Kanatzidis, M. G., Laser Scribing for Electrode Patterning of Perovskite Spectrometer-Grade CsPbBr3 Gamma-ray Detectors. *ACS Applied Materials & Interfaces* **2023,** 15, (13), 16895-16901.
26. Song, S.; Yoon, A.; Jang, S.; Lynch, J.; Yang, J.; Han, J.; Choe, M.; Jin, Y. H.; Chen, C. Y.; Cheon, Y.; Kwak, J.; Jeong, C.; Cheong, H.; Jariwala, D.; Lee, Z.; Kwon, S.-Y., Fabrication of p-type 2D single-crystalline transistor arrays with Fermi-level-tuned van der Waals semimetal electrodes. *Nature Communications* **2023,** 14, (1), 4747.
27. Besleaga, C.; Abramiuc, L. E.; Stancu, V.; Tomulescu, A. G.; Sima, M.; Trinca, L.; Plugaru, N.; Pintilie, L.; Nemnes, G. A.; Iliescu, M.; Svavarsson, H. G.; Manolescu, A.; Pintilie, I., Iodine Migration and Degradation of Perovskite Solar Cells Enhanced by Metallic Electrodes. *The Journal of Physical Chemistry Letters* **2016,** 7, (24), 5168-5175.
28. Shrestha, S.; Tsai, H.; Yoho, M.; Ghosh, D.; Liu, F.; Lei, Y.; Tisdale, J.; Baldwin, J.; Xu, S.; Neukirch, A. J.; Tretiak, S.; Vo, D.; Nie, W., Role of the Metal–Semiconductor Interface in Halide Perovskite Devices for Radiation Photon Counting. *ACS Applied Materials & Interfaces* **2020,** 12, (40), 45533-45540.
29. Maculan, G.; Sheikh, A. D.; Abdelhady, A. L.; Saidaminov, M. I.; Haque, M. A.; Murali, B.; Alarousu, E.; Mohammed, O. F.; Wu, T.; Bakr, O. M., CH3NH3PbCl3 Single Crystals: Inverse Temperature Crystallization and Visible-Blind UV-Photodetector. *The Journal of Physical Chemistry Letters* **2015,** 6, (19), 3781-3786.
30. Saidaminov, M. I.; Abdelhady, A. L.; Murali, B.; Alarousu, E.; Burlakov, V. M.; Peng, W.; Dursun, I.; Wang, L.; He, Y.; Maculan, G.; Goriely, A.; Wu, T.; Mohammed, O. F.; Bakr, O. M., High-quality bulk hybrid perovskite single crystals within minutes by inverse temperature crystallization. *Nature Communications* **2015,** 6, (1), 7586.
31. Wang, X.; Huang, Y.; Lei, W.; Li, Q.; Zhang, X.; Khan, Q.; Wang, B., Asymmetrical Photodetection Response of Methylammonium Lead Bromide Perovskite Single Crystal. *Crystal Research and Technology* **2017,** 52, (9), 1700115.
32. Berger, M. J. et al. XCOM: Photon Cross Sections Database: NIST Standard Reference Database 8 (NIST, 2013); https://www.nist.gov/pml/xcom-photoncross-sections-database